860 *Inorg. Chem.* **2010**, *49*, 860–869
DOI: 10.1021/ic901194k

Inorganic Chemistry
Article

Oxidation State Characterization of Ruthenium 2−Iminoquinone Complexes through Experimental and Theoretical Studies

Jonathan Rochford,[†,§] Ming-Kang Tsai,[†] David J. Szalda,[∥] Julie L. Boyer,[†] James T. Muckerman,[†,‡] and Etsuko Fujita*[,†]

[†]*Chemistry Department, Brookhaven National Laboratory, Upton, New York 11973-5000,* [‡]*Center for Functional Nanomaterials, Brookhaven National Laboratory, Upton, New York 11973-5000, and* [∥]*Department of Natural Sciences, Baruch College, New York, New York 10010.* [§]*Current address: Department of Chemistry, University of Massachusetts, 100 Morrisey Boulevard, Boston, MA 02125.*

Received June 22, 2009

The synthesis of complexes $[Ru^{II}(trpy)(2\text{-imino-4-}tert\text{-butylquinone})(Cl)]^+$ and $[Ru^{II}(trpy)(NIL)(OAc)]^+$ (where trpy = 2:2′,6′:2″-terpyridyl, NIL = 2-imino-4-*tert*-butylquinone, 2-imino-4-methylquinone, 2-iminoquinone, 2-imino-4-chloroquinone, 2-imino-5-chloroquinone, 2-imino-4,6-di-*tert*-butyl-*N*-phenyl-quinone, 2-imino-4,6-di-*tert*-butyl-*N*-(2′-trifluoromethylphenyl)-quinone) is reported. The oxidation states of these complexes, as well as the previously reported $[Ru^{III}(trpy)(2\text{-iminosemiquinone})(Cl)]^+$ complex, are investigated by spectroscopic, electrochemical and theoretical methods resulting in the latter complex being reassigned as $[Ru^{II}(trpy)(2\text{-iminoquinone})(Cl)]^+$. Evidence for the presence of two structural isomers was found for all complexes, and crystal structures for both isomers of the $[Ru^{II}(trpy)(2\text{-imino-4-}tert\text{-butylquinone})(Cl)]ClO_4$ complex are reported, as well as for the *cis* isomer of $[Ru^{II}(trpy)(2\text{-imino-4,6-di-}tert\text{-butyl-}N\text{-phenyl-quinone})(OAc)]PF_6$. Redox control is also demonstrated based on the Hammett parameters of the substituents on the 2-iminoquinone ligand.

Introduction

Transition-metal complexes with redox-active, or *non-innocent*, ligands (NILs) have generated much interest in recent years owing to an increased curiosity about the prospective role of various ligand-based oxidation states in either stoichiometric or catalytic molecular transformations.[1−10] Such interest is evidenced by the dedication of a highly informative symposium on the topic at a recent national ACS meeting.[11] The description *non-innocent* derives from the statement by Jørgensen over 40 years ago that "*ligands are innocent when they allow oxidation states of the central atoms to be defined.*"[12] The term *non-innocent*, often used interchangeably with "redox-active," is therefore used when the ligand(s) in a metal complex have significant consequences on the electrochemistry of the complex as a whole *and* undergo redox chemistry themselves. There are many examples of NILs of various geometric and electronic structures used in an assortment of environments with metal centers from across the periodic table. In addition to dioxolene[13−16] ligands and their imino analogues, nitrosyl,[17,18] dithiolene,[19] polypyridyl,[20] and porphyrinogens[21] are just a

*To whom correspondence should be addressed. E-mail: fujita@bnl.gov.

(1) Wada, T.; Tsuge, K.; Tanaka, K. *Chem. Lett.* **2000**, 910–911.
(2) Wada, T.; Tsuge, K.; Tanaka, K. *Angew. Chem., Int. Ed.* **2000**, *39*, 1479–1482.
(3) Hino, T.; Wada, T.; Fujihara, T.; Tanaka, K. *Chem. Lett.* **2004**, *33*, 1596–1597.
(4) Miyazato, Y.; Wada, T.; Tanaka, K. *Bull. Chem. Soc. Jpn.* **2006**, *79*, 745–747.
(5) Miyazato, Y.; Wada, T.; Muckerman, J. T.; Fujita, E.; Tanaka, K. *Angew. Chem., Int. Ed.* **2007**, *46*, 5728–5730.
(6) Blackmore, K. J.; Sly, M. B.; Haneline, M. R.; Ziller, J. W.; Heyduk, A. F. *Inorg. Chem.* **2008**, *47*, 10522–10532.
(7) Muckerman, J. T.; Polyansky, D. E.; Wada, T.; Tanaka, K.; Fujita, E. *Inorg. Chem.* **2008**, *47*, 1787–1802.
(8) Ringenberg, M. R.; Kokatam, S. L.; Heiden, Z. M.; Rauchfuss, T. B. *J. Am. Chem. Soc.* **2008**, *130*, 788–789.
(9) Chaudhuri, P.; Verani, C. N.; Bill, E.; Bothe, E.; Weyhermuller, T.; Wieghardt, K. *J. Am. Chem. Soc.* **2001**, *123*, 2213–2223.
(10) Bouwkamp, M. W.; Bowman, A. C.; Lobkovsky, E.; Chirik, P. J. *J. Am. Chem. Soc.* **2006**, *128*, 13340.
(11) Guilty Pleasures: The Joys of Metal Complexes of Non-Innocent, Redox-Active Ligands, Proceedings of the 236th American Chemical Society National Meeting and Exposition, Philadelphia, PA, U.S.A., August 17th−21st, 2008.
(12) Jørgensen, C. K. *Coord. Chem. Rev.* **1966**, *1*, 164–178.
(13) Pierpont, C. G.; Buchanan, R. M. *Coord. Chem. Rev.* **1981**, *38*, 45–87.
(14) Pierpont, C. G. *Coord. Chem. Rev.* **2001**, *219*, 415–433.
(15) Zanello, P.; Corsini, M. *Coord. Chem. Rev.* **2006**, *250*, 2000–2022.
(16) Pierpont, C. G.; Lange, C. W. In *Progress in Inorganic Chemistry*; Karlin, K. D., Ed.; John Wiley & Sons, Inc.: Hoboken, NJ, 2007; pp 331−442.
(17) McCleverty, J. A. *Chem. Rev.* **2004**, *104*, 403–418.
(18) Das, A. K.; Sarkar, B.; Duboc, C.; Strobel, S.; Fiedler, J.; Záliš, S.; Lahiri, G. K.; Kaim, W. *Angew. Chem., Int. Ed.* **2009**, *48*, 4242–4245.
(19) Sugimoto, H.; Tsukube, H. *Chem. Soc. Rev.* **2008**, *37*, 2609–2619.
(20) Juris, A.; Balzani, V.; Barigelletti, F.; Campagna, S.; Belser, P.; Vonzelewsky, A. *Coord. Chem. Rev.* **1988**, *84*, 85–277.
(21) In *The Porphyrin Handbook*; Kadish K. M., Guilard, R., Eds.; Academic Press: New York, 1999; Vol. *9*.

 Published on Web 12/28/2009

Scheme 1. Resonance Structures of Class A, B, C, and D with Various Oxidation States of Ru−NIL Type Complexes[a]

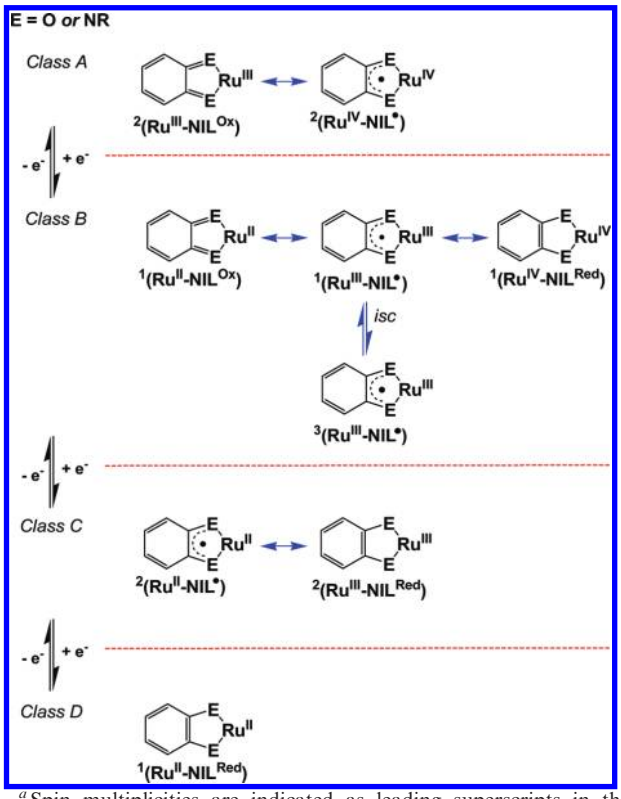

[a] Spin multiplicities are indicated as leading superscripts in the oxidation state designations.[30] Possible intersystem crossing between singlet and triplet states is indicated by "isc".

few examples of other ligands known to exhibit non-innocent behavior. For the remainder of this paper, however, we will use only the NIL designation in reference to the quinone, 2-iminoquinone, or benzoquinonediimine frameworks with their oxidation states indicated by a superscript (Scheme 1). Ru−NIL complexes which possess strong Ru(dπ)−NIL(π*) metal−ligand interactions due to (near-) degenerate mixing are of special interest.[22−26] This strong interaction results in extensive delocalization of electron density over the Ru−NIL π-network that is very sensitive to the energies of the NIL π* orbitals. In fact, the Ru−NIL system has previously been described as a fully delocalized aromatic 5-membered ring system incorporating the metal center, both heteroatoms and their α-carbons.[27−29] As a result of this high sensitivity, the charge distribution between the metal center and the ligand can be modulated depending on the nature of the ligand substituents and is often expressed in terms of resonance structures as, NILs can exist in NIL^{Ox}, $NIL^{\bullet}$, or NIL^{Red} forms (Scheme 1).

The assignment of oxidation states and spin states for these systems, however, is not trivial and is often ambiguous for Class B systems, a subject which has been discussed in detail in a recent review article.[26] Relevant to this study is the characterization of oxidation states for the Class B species $[Ru(trpy)(3,5\text{-}^tBu_2C_6H_2O_2)(OH)]^+$ whose ground state has been assigned as principally a closed-shell singlet $Ru^{II}-NIL^{Ox}$ configuration.[7,25] This example is of significance because $[Ru(trpy)(3,5\text{-}^tBu_2C_6H_2O_2)(OH)]^+$ is isoelectronic with the chloride and acetate systems investigated here. A detailed analysis of density functional theory (DFT)-calculated structures, spin densities, and **g**-tensor anisotropies led to ambiguous (i.e., intermediate) assignments for a series of $[Ru(NIL)(acac)_2]^{-,0,+}$ complexes with different NIL.[31] In a recent study of Class C $[Ru(NIL)(trpy)(OAc)]^0$ dioxolene complexes by Wada et al., the electron paramagnetic resonance (EPR) spectra showed increased anisotropy with increasing strength of the electron withdrawing substituent of the NIL.[32] It was demonstrated that resonance between the $Ru^{II}-NIL^{\bullet}$ and $Ru^{III}-NIL^{Red}$ frameworks could be controlled by the electron donating or withdrawing strength of the NIL substituent. DFT calculations showed an increase in Ru^{III} character with an increase in the electron withdrawing strength of substituents on the NIL ligand thus favoring the NIL^{Red} oxidation state. This effect was explained by a decrease in the energy of the singly occupied molecular orbital (SOMO) of $NIL^{\bullet}$. It was concluded that the electron configuration of these complexes can be described as predominantly $Ru^{II}-NIL^{\bullet}$ with the contribution of $Ru^{III}-NIL^{Red}$ increasing as the strength of the electron withdrawing substituents on the NIL increases.

Of particlular relevance to the present work is a recent report by Maji et al. in which the Class B complexes $[Ru(trpy)(C_6H_4NHO)(Cl)]^+$ and $[Ru(trpy)(C_6H_4NHNH)(Cl)]^+$ were reported.[33] Both complexes were assigned as having an open-shell, singlet-coupled $Ru^{III}-NIL^{\bullet}$ electron configuration on the basis of theoretical (DFT) and experimental (X-ray crystallography) bond lengths. Assignment of oxidation states for such Ru−NIL systems based on X-ray data, however, often leads to invalid interpretation.[26] Theoretical analysis of Class B systems, including $[Ru(trpy)(C_6H_4NHO)(Cl)]^+$ and $[Ru(trpy)(C_6H_4NHNH)(Cl)]^+$, may also lead to mistaken assignments. Standard DFT calculations often erroneously predict a triplet ground state, and in such cases it requires a Broken-Symmetry (BS) calculation to demonstrate that an antiferromagnetically coupled, open-shell singlet state has a lower energy than the ferro-magnetically coupled triplet state. In the theoretical treatment of the nine related Class B complexes considered here (as discussed below), including the two studied previously be Maji et al.,[33] all attempts to converge an open-shell singlet-coupled configuration $Ru^{III}-NIL^{\bullet}$ using the BS-DFT approach collapsed to the closed-shell singlet $Ru^{II}-NIL^{Ox}$ configuration.

(22) Lever, A. B. P.; Masui, H.; Metcalfe, R. A.; Stufkens, D. J.; Dodsworth, E. S.; Auburn, P. R. *Coord. Chem. Rev.* **1993**, *125*, 317–331.
(23) Gorelsky, S. I.; Dodsworth, E. S.; Lever, A. B. P.; Vlcek, A. A. *Coord. Chem. Rev.* **1998**, *174*, 469–494.
(24) Lever, A. B. P.; Gorelsky, S. I. *Optical Spectra and Chemical Bonding in Transition Metal Complexes*: Special Volume *II*; Springer: New York, 2004; Vol. II, Structure and Bonding, p 107.
(25) Tsai, M.-K.; Rochford, J.; Polyansky, D. E.; Wada, T.; Tanaka, K.; Fujita, E.; Muckerman, J. T. *Inorg. Chem.* **2009**, *48*, 4372–4383.
(26) Boyer, J. L.; Rochford, J.; Tsai, M.-K.; Muckerman, J. T.; Fujita, E. *Coord. Chem. Rev.* **2010**, *254*, 309−330.
(27) Masui, H. *Coord. Chem. Rev.* **2001**, *219−221*, 957–992.
(28) Milcic, M. K.; Ostojic, B. D.; Zaric, S. D. *Inorg. Chem.* **2007**, *46*, 7109–7114.
(29) Beaulac, R.; Lever, A. B. P.; Reber, C. *Eur. J. Inorg. Chem.* **2007**, *2007*, 48–52.
(30) For Class B systems, resonance is only spin-allowed for the singlet states. Formation of a Class B system, via reduction of a Class I species or oxidation of a Class C species, can result in the singlet or triplet open-shell states depending on the co-ligands involved.
(31) Remenyi, C.; Kaupp, M. *J. Am. Chem. Soc.* **2005**, *127*, 11399–11413.
(32) Wada, T.; Yamanaka, M.; Fujihara, T.; Miyazato, Y.; Tanaka, K. *Inorg. Chem.* **2006**, *45*, 8887–8894.
(33) Maji, S.; Patra, S.; Chakraborty, S.; Janardanan, D.; Mobin, S. M.; Sunoj, R. B.; Lahiri, G. K. *Eur. J. Inorg. Chem.* **2007**, 314–323.

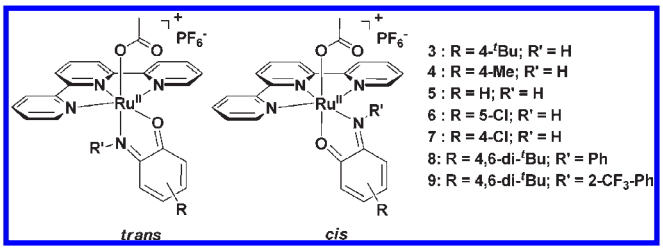

Figure 1. Structures of $[Ru^{II}(trpy)(NIL^{Ox})(OAc)]^+$ complexes.

We therefore believe the species reported by Maji et al. to be closer to a $[Ru^{II}(trpy)(NIL^{Ox})(Cl)]^+$ configuration based on the analysis presented below. In this paper we describe experimental and theoretical studies on the electronic structures of a series of Class B ruthenium complexes $[Ru(trpy)(NIL)(X)]^+$ (X = Cl^- or OAc^-) having various substituents on the 2-iminoquinone NIL ligand (Figure 1). The Class C, one-electron-reduced analogues were prepared in situ by controlled potential electrolysis and monitored by UV−vis absorption spectroscopy. By using a combination of electrochemical, spectroscopic, X-ray crystallographic, and theoretical methods, a better understanding of electronic structures is achieved for these systems.

Experimental Section

Synthesis. Tetrabutylammonium hexafluorophosphate (Bu_4NPF_6), potassium acetate, 2-aminophenol, 2-amino-4-*tert*-butylphenol, 2-amino-4-methylphenol, 2-amino-4-chlorophenol, 2-amino-5-chlorophenol, methanol (reagent grade), acetone (reagent and spectrophotometric grades), diethyl ether (reagent grade), alumina (neutral, activated) were all used as received from Aldrich. The ligands 2-anilino-4,6-di-*tert*butylphenol and 2-(2-trifluoromethyl)anilino-4,6-di-*tert*-butylphenol were prepared according to literature methods.[9,34]

The chloride complexes $[Ru(trpy)(C_6H_4NHO)(Cl)][PF_6]$ (**1**) and $[Ru(trpy)(4\text{-}^tBuC_6H_3NHO)(Cl)][PF_6]$ (**2**) were prepared following a previously reported procedure, complex **1** being in good agreement with the previously reported data [NB: only one isomer was previously reported whereas this study finds a mixture of two isomers].[33] Acetate complexes (**3**−**9**) were prepared by a modification of a known procedure for neutral dioxolene Class C $[Ru^{II}(trpy)(NIL^{\bullet})(OAc)]^0$ type complexes.[32] We note that although the latter dioxolene species are generally stable on silica gel or alumina, their 2-iminoquinone analogues decompose readily. Decomposition occurs slower on alumina thus flash chromatography using a short plug column proved successful.

$[Ru(trpy)(4\text{-}^tBuC_6H_3NHO)(Cl)][PF_6]$ (2). 97 mg, 63%. UV−vis (acetone) λ_{max}: 567 nm (1.55×10^4 M^{-1} cm^{-1}). ESI-MS (*m*/*z*): calcd. 533.1; *m*/*z* obs. 533.1. Elemental analysis for $C_{25}H_{24}ClF_6N_4OPRu \cdot 2H_2O$: calcd C 42.05%; H 3.95%; N 7.85%; obs. C 41.55%; H 4.07%; N 7.67%.

General Procedure for Preparation of [Ru(trpy)(NIL)(OAc)][PF_6] Complexes (3−9). A 200 mL flask was charged with 100 mL of methanol, and the solution was purged with argon for 20 min. Addition of 0.46 mmol (200 mg) $Ru(trpy)Cl_3$ and 0.46 mmol of the appropriate 2-aminophenol resulted in a deep brown suspension. An excess of potassium acetate, 400 mg (4 mmol), was then added affording a deep purple solution. The solution was left stirring under argon for 3 days after which time the volume of methanol was reduced under vacuum to about 2−3 mL. The complete conversion from $Ru^{II}(trpy)(NIL^{\bullet})(OAc)$ to $Ru^{II}(trpy)(NIL)(OAc)^+$ can be achieved by the following workup procedure performed in air. Addition of 100 mL of acetone resulted in the precipitation of the excess potassium acetate which was subsequently removed by filtration. The deep purple filtrate was then reduced to 10 mL under vacuum, and the PF_6 salt was precipitated by addition of 10 mL of 1 M aqueous NH_4PF_6. Further product could be recovered by careful removal of the acetone under vacuum. The precipitate was collected by Buchner filtration and washed with diethyl ether. The solid was then dissolved in a minimum volume of an acetone/methanol solvent mixture (v/v 95/5) and was quickly flashed through a short alumina plug column (ca. 2 cm length activated, neutral alumina) using an acetone/methanol solvent mixture (v/v 95/5). After collection of the deep magenta colored fraction, the solvent was reduced to about 5 mL under vacuum, and addition of diethyl ether resulted in precipitation of a dark purple powder. The solid was filtered and dried under vacuum. Complexes **8** and **9** were prepared in a similar manner with the exception that chromatography was not needed for purification. Complexes $\mathbf{3}^-$−$\mathbf{9}^-$ were prepared by the in situ electrochemical method.

$[Ru^{II}(trpy)(4\text{-}^tBuC_6H_3NHO)(OAc)][PF_6]$ (3). 187 mg, 58%. UV−vis (acetone) λ_{max}: 565 nm (1.69×10^4 M^{-1} cm^{-1}). ESI-MS (*m*/*z*): calcd 557.1; obs. 557.1. Elemental analysis for $C_{27}H_{27}F_6N_4O_3PRu \cdot H_2O$: calcd C 45.05%; H 4.06%; N 7.79%; obs. C 44.55%; H 3.32%; N 8.00%.

$Ru(trpy)(4\text{-}^tBuC_6H_3NHO)(OAc)$ (3^-). UV−vis (acetone/0.1 M Bu_4NPF_6) λ_{max}: 708 nm (1.05×10^4 M^{-1} cm^{-1}).

$[Ru(trpy)(4\text{-}MeC_6H_3NHO)(OAc)][PF_6]$ (4). 140 mg, 46%. UV−vis (acetone) λ_{max}: 566 nm (1.61×10^4 M^{-1} cm^{-1}). ESI-MS (*m*/*z*): calcd. 515.1; obs. 515.0. Elemental analysis for $C_{24}H_{21}F_6N_4O_3PRu \cdot 2H_2O$: calcd C 41.45%; H 3.62%; N 8.06%; obs. C 40.98%; H 3.26%; N 7.78%.

$Ru(trpy)(4\text{-}MeC_6H_3NHO)(OAc)$ (4^-). UV−vis (acetone/0.1 M Bu_4NPF_6) λ_{max}: 710 nm (1.04×10^4 M^{-1} cm^{-1}).

$[Ru(trpy)(C_6H_4NHO)(OAc)][PF_6]$ (5). 150 mg, 50%. UV−vis (acetone) λ_{max}: 553 nm (1.70×10^4 M^{-1} cm^{-1}). ESI-MS (*m*/*z*): calcd. 501.1; obs. 500.9. Elemental analysis for $C_{23}H_{19}F_6N_4O_3PRu$: calcd C 42.80%; H 2.97%; N 8.68%; obs. C 43.34%; H 3.38%; N 8.65%.

$Ru(trpy)(C_6H_4NHO)(OAc)$ (5^-). UV−vis (acetone/0.1 M Bu_4NPF_6) λ_{max}: 706 nm (1.49×10^4 M^{-1} cm^{-1}).

$[Ru^{II}(trpy)(5\text{-}ClC_6H_3NHO)(OAc)][PF_6]$ (6). 144 mg, 43%. UV−vis (acetone) λ_{max}: 553 nm (1.83×10^4 M^{-1} cm^{-1}). ESI-MS (*m*/*z*): calcd. 535.0; obs. 534.8. Elemental analysis for $C_{23}H_{18}ClF_6N_4O_3PRu \cdot H_2O$: calcd C 39.56%; H 2.89%; N 8.03%; obs. C 38.99%; H 2.51%; N 8.01%.

$Ru^{II}(trpy)(5\text{-}ClC_6H_3NHO)(OAc)$ (6^-). UV−vis (acetone/0.1 M Bu_4NPF_6) λ_{max}: 716 nm (1.23×10^4 M^{-1} cm^{-1}).

$[Ru^{II}(trpy)(4\text{-}ClC_6H_3NHO)(OAc)][PF_6]$ (7). 136 mg, 46%. UV−vis (acetone) λ_{max}: 559 nm (1.51×10^4 M^{-1} cm^{-1}). ESI-MS (*m*/*z*): calcd. 535.0; obs. 534.9. Elemental analysis for $C_{23}H_{18}ClF_6N_4O_3PRu \cdot H_2O$: calcd C 39.56%; H 2.89%; N 8.03%; obs. C 39.28%; H 2.63%; N 8.11%.

$Ru^{II}(trpy)(4\text{-}ClC_6H_3NHO)(OAc)$ (7^-). UV−vis (acetone/0.1 M Bu_4NPF_6) λ_{max}: 720 nm (1.21×10^4 M^{-1} cm^{-1}).

$[Ru^{II}(trpy)(4,6\text{-}^tBu_2C_6H_2N(Ph)O)(OAc)][PF_6]$ (8). 112 mg, 67%. UV−vis (acetone) λ_{max}: 568 nm (1.92×10^4 M^{-1} cm^{-1}). ESI-MS (*m*/*z*): calcd. 689.2; obs. 689.0. Elemental analysis for $C_{37}H_{39}F_6N_4O_3PRu \cdot H_2O$: calcd 52.15%; H 4.85%; N 6.58%; obs C 51.65%; H 4.37%; N 6.78%.

$Ru^{II}(trpy)(4,6\text{-}^tBuC_6H_3N(Ph)O)(OAc)$ (8^-). UV−vis (acetone/0.1 M Bu_4NPF_6) λ_{max}: 720 nm (1.60×10^4 M^{-1} cm^{-1}).

$[Ru^{II}(trpy)(4,6\text{-}^tBu_2C_6H_3N(2\text{-}CF_3Ph)O)(OAc)][PF_6]$. (9). 77 mg, 45%. UV−vis (acetone) λ_{max}: 562 nm (1.73×10^4 M^{-1} cm^{-1}). ESI-MS (*m*/*z*): calcd. 757.2; obs. 757.1. Elemental

(34) Eckhard, B.; Bothe, E.; Chaudhuri, P.; Chlopek, K.; Herebian, D.; Kokatam, S.; Ray, K.; Weyhermüller, T.; Neese, F.; Wieghardt, K. *Chem.—Eur. J.* **2005**, *11*, 204–224.

analysis for $C_{38}H_{38}F_9N_4O_3PRu \cdot H_2O$: calcd C 49.60%; H 4.39%; N 6.09%; obs C 49.49%; H 4.26%; N 6.06%.

Ru^{II}(trpy)(4,6-^{t}Bu$_2$C$_6$H$_3$N(2-CF$_3$Ph)O)(OAc) (9$^-$). UV−vis (acetone/0.1 M Bu_4NPF_6) λ_{max}: 730 nm (1.58×10^4 M^{-1} cm^{-1}).

Physical Measurements. UV−vis absorption spectra were recorded on a Hewlett-Packard 8452A diode array spectrophotometer in spectrophotometric grade acetone. ^{1}H NMR spectra were recorded on a Bruker UltraShield 400 MHz spectrometer in d_6-acetone (Cambridge Isotopes). ESI-MS was carried out on a Thermo Finnigan mass spectrometer. Cyclic and square-wave voltammetry experiments were both carried out on a BAS100 electrochemical system in a standard three electrode cell under an atmosphere of argon in a 0.1 M Bu_4NPF_6 acetone electrolyte. Glassy carbon (3 mm diameter) and Pt wire were used as working and counter electrodes, respectively. A homemade organic reference electrode consisting of a Ag wire in a 1 mM $AgNO_3$/0.1 M Bu_4NPF_6 acetonitrile electrolyte (measured at +349 mV vs a BAS Ag/AgCl 3 M aqueous KCl) was used to reduce any junction potential issues. The ferrocene/ferricinium redox couple (+ 450 mV vs Ag/AgCl in a 0.1 M Bu_4NPF_6 acetonitrile electrolyte) was used as an internal standard for calibration purposes. All voltammetry measurements were carried out using the open-circuit potential *or* "rest potential" (V_{oc}) as the initial potential. The half-wave potential, $E_{1/2}$, was determined from cyclic voltammetry as $(E_{pa} + E_{pc})/2$, where E_{pa} and E_{pc} are the anodic and cathodic peak potentials, respectively. It is assumed that $E_{1/2} \cong E^0$ for all measurements, that is, differences between diffusion coefficients of oxidized and reduced species are considered negligible. Where $E_{1/2}$ could not be calculated because of the irreversible metal-centered oxidation, potentials are reported from square-wave voltammograms (step: 4 mV, amplitude: 10 mV, frequency: 15 s^{-1}). Redox couples were only designated as fully reversible processes after an in-depth scan-rate dependence study. These electrochemical results are summarized in Table 1. Bulk electrolysis experiments were carried out in a custom-made flow cell with Pt-mesh working and counter electrodes.[35] The one-electron stoichiometry of the electrolysis products was confirmed by controlled potential electrolysis with applied potentials 200 mV negative of the respective redox couple ensuring an equilibrium of > 1000:1 of reduced:oxidized species. Hammett plots of $E_{1/2}$ versus σ, where σ is the Hammett constant, were constructed using previously reported σ values and are here taken as *meta* and *para* with respect to the C=O group of the 2-ImQ ligand.[36]

X-ray Crystallography. Collection and Reduction of X-ray Data for 2c, 2t, and 8c.[37] All crystals were grown at room temperature by vapor diffusion of ether into an acetone solution of the complex. In looking at crystals of [Ru(trpy)(4-^{t}BuC$_6$H$_3$NHO)(Cl)]ClO_4, two crystal forms were observed. Larger, thicker plate shaped crystals and smaller, thinner plates. The compound was known to have two possible structural isomers so crystals of each form were studied. X-ray data sets were collected on crystals of [Ru(trpy)(4-^{t}BuC$_6$H$_3$NHO)Cl]$ClO_4 \cdot CH_3CN$ (**2t**), and [Ru(trpy)(4-^{t}BuC$_6$H$_3$NHO)(Cl)]ClO_4 (**2c**). Crystals of **2t** were cut and then coated with Vaseline and sealed inside a glass capillary which was then transferred to an Enraf Nonius CAD-4 diffractometer for the collection of diffraction data. Crystals of (**2c**) were mounted on a loop and studied on an Oxford Gemini A Ultra diffractometer at 100 K. Crystals of [Ru(trpy)(4,6-^{t}Bu$_2$C$_6$H$_2$-N(Ph)O)(OAc)]$PF_6 \cdot (H_2O)$ (**8c**) were mounted on the end of a glass fiber and transferred to an Enraf Nonius CAD-4 diffractometer for the collection of diffraction data. Diffraction data for all three crystals indicated triclinic symmetry consistent with space group $P\bar{1}$. Crystal data and information about the data collection are provided in Table 2 and Supporting Information, Table S1.

Table 1. Electrochemical Data for Complexes **1**−**9** Recorded in Acetone (0.1 M Bu_4NPF_6) at a Glassy Carbon Working Electrode with Scan Rate of 50 mV s^{-1}

		$E_{1/2}$ (V vs Ag/AgCl)			
		oxidation[a]		reduction	
	V_{oc} (V)	$Ru^{IV/III}$	$Ru^{III/II}$	$NIL^{Ox/\bullet}$	$NIL^{\bullet/Red}$
1	+0.06	+1.41	+1.17	−0.21	−1.02
2	+0.10	+1.38	+1.19	−0.27	−1.05
3	+0.08	+1.28	+1.13	−0.23	−1.01
4	+0.13	+1.26	+1.14	−0.21	−1.01
5	+0.11	∼	+1.15	−0.17	−0.98
6	+0.13	∼	+1.26	−0.07	−0.89
7	+0.14	∼	+1.38	−0.06	−0.89
8	+0.02	+1.45	+1.27	−0.19	−1.02
9	+0.07	+1.50	+1.38	−0.14	−1.02

[a] $Ru^{III/II}$ and $Ru^{IV/III}$ oxidation potentials for complexes **1**−**8** are estimated from square-wave voltammetry experiments because of the irreversible nature of these redox couples.

Determination and Refinement of the Structures. The structure of **2t** was solved by standard heavy atom Patterson methods while **2c** and **8c** were solved by direct methods.[38] Space group $P\bar{1}$ was used for the solution and refinement of *all three structures*. In the least-squares refinement,[38] anisotropic temperature parameters were used for all the non-hydrogen atoms. Hydrogen atoms were placed at calculated positions and allowed to "ride" on the atom to which they were attached. A common isotropic thermal parameter was refined for the hydrogen atoms in each structure. For **2t** and **8c** the data were corrected using a Fourier absorption correction (XABS2)[39] while for **2c** an analytical absorption correction using face indexing was applied.

Computational Details. All calculations were carried out using DFT with the B3LYP functional as implemented in the Gaussian 03 program package. The SDD (i.e., MWB28) effective core potential and basis set were used for Ru,[40] and the 6-31G* basis set for all other atoms.[41,42] A vibrational frequency analysis was carried out to confirm the minimum-energy geometry and to determine the thermal correction, that is, zero-point energy (ZPE), translational/rotational/vibrational energies, and entropy, for each species under the perfect gas, rigid rotor, and harmonic oscillator approximations. Mulliken atomic charges were also calculated at the gas-phase optimized geometry. Wave function stability tests were carried out to validate the convergence of the electronic wave function calculation. The solvation effect was treated by the CPCM polarizable continuum model with UAKS radii and acetone as solvent.[43,44] Time-dependent density functional theory combined with the CPCM solvation model was used to calculate UV−vis spectra at the gas-phase optimized geometries. All of the electronic structure calculations were carried out with Gaussian 03 program.[45]

(35) Fajer, J.; Fujita, I.; Davis, M. S.; Forman, A.; Smith, K. M. *Electrochemical and Spectrochemical Studies of Biological Redox Components; Adv. Chem. Ser. 201*; American Chemical Society: Washington, DC, 1982; Vol. 201.
(36) Brown, H. C.; Okamoto, Y. *J. Am. Chem. Soc.* **1958**, *80*, 4979–4987.
(37) 'c' and 't' represent cis and trans isomers, respectively.
(38) Sheldrick, G. M. *SHELXTL*, 5th ed.; Siemens Analytical Instruments Inc.: Madison, WI, 1994.
(39) Parkin, S. M. B.; Hope, H. *J. Appl. Crystallogr.* **1995**, *28*, 53–56.
(40) Andrae, D.; Haeussermann, U.; Dolg, M.; Stoll, H.; Preuss, H. *Theor. Chim. Acta* **1990**, *77*, 123–141.
(41) Hariharan, P.; Pople, J. A. *Theor. Chim. Acta* **1973**, *28*, 213–222.
(42) Francl, M. M.; Pietro, W. J.; Hehre, W. J.; Binkley, J. S.; Gordon, M. S.; Defrees, D. J.; Pople, J. A. *J. Chem. Phys.* **1982**, *77*, 3654–3665.
(43) Barone, V.; Cossi, M. *J. Phys. Chem. A* **1998**, *102*, 1995–2001.
(44) Cossi, M.; Rega, N.; Scalmani, G.; Barone, V. *J. Comput. Chem.* **2003**, *24*, 669–681.
(45) Frisch, M. J. et al. *Gaussian 03*, D.01; Gaussian Inc.: Wallingford, CT, 2004.

Table 2. Crystallographic Collection and Refinement Data[a]

	2t	2c	8c
formula	$C_{27}H_{27}Cl_2N_5O_5Ru$	$C_{25}H_{24}Cl_2N_4O_5Ru$	$C_{37}H_{41}F_6N_4O_4PRu$
fw	673.51	632.45	851.78
temp (K)	293(2)	100 (2)	293(2)
cryst. syst	triclinic	triclinic	triclinic
space group	$P\bar{1}$ (No. 2)	$P\bar{1}$ (No. 2)	$P\bar{1}$ (No. 2)
a (Å)	8.809(3)	9.814(5)	10.664(4)
b (Å)	11.935(4)	10.816(5)	11.666(5)
c (Å)	14.840(5)	13.437(5)	16.705(10)
α (deg)	90.14(3)	95.932(5)	88.67(5)
β (deg)	93.67(3)	107.124(5)	72.85(4)
γ (deg)	111.37(3)	101.968(5)	77.20(3)
V (Å^3)	1449.4(8)	1312.7(10)	1934.5(16)
Z	2	2	2
μ	6.459 mm^{-1}	7.078 mm^{-1}	4.304 mm^{-1}
λ (Å)	1.54178	1.54178	1.54178
ρ calc (g cm^{-3})	1.541	1.600	1.462
cryst. size (mm)	0.20 × 0.20 × 0.20	0.26 × 0.18 × 0.07	0.25 × 0.17 × 0.10
θ range (deg)	2.98 to 72.65	3.50 to 58.92	2.98 to 72.65
total no. of reflns	5699	2968	7252
no. of independent reflns $I \geq 3.0\sigma$(I)	2917	2537	7252
no. of parameters	362	332	479
final R indices [$I > 3\sigma(I)$]	R1 = 0.0706, wR2 = 0.1864	R1 = 0.0950, wR2 = 0.2313	R1 = 0.0693, wR2 = 0.1638
R indices (all data)	R1 = 0.2070, wR2 = 0.2324	R1 = 0.1110, wR2 = 0.2465	R1 = 0.2925, wR2 = 0.2258
Goodness-of-fit on F^2	1.048	1.041	0.981
extinction coefficient	none	none	none
absorption correction	Fourier(XABS2)[a]	analytical	empirical

[a] $R1 = \sum||F_o| - |F_c||/\sum|F_o|$; $wR2 = \{\sum w(F_o^2 - F_c^2)^2/\sum w(F_o^2)^2\}^{1/2}$.

Scheme 2. Preparation of Ru^{II}(trpy)(NIL)(OAc)$^+$

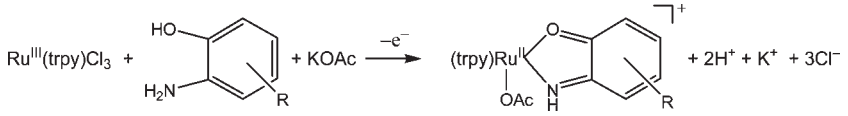

Results and Discussion

Synthesis. Complex **1** was synthesized as previously reported, and the 4-*tert*-butyl derivative **2** was prepared by a similar procedure.[33] The acetate complexes **3**−**9** were prepared by adapting a previously reported procedure for Class C dioxolene [Ru(trpy)(NIL)(OAc)]^0 complexes by stirring Ru(trpy)Cl_3, 1 equiv of the appropriate 2-aminophenol, and a 9-fold excess of potassium acetate in methanol at room temperature under argon for 3 days.[32] The oxidized Class B analogue [Ru(trpy)(NIL)(OAc)]$^+$ was isolated (Scheme 2), most likely because of the lower oxidation potential of the 2-amidophenolate ligand with respect to the catecholate ligand. While the source of the oxidant is not clear, we believe leaked air may have contributed to the formation of Ru^{II}(trpy)(NIL)(OAc)$^+$ from Ru^{II}(trpy)(NIL$^{\bullet}$)(OAc), which is an air-sensitive species.

Although an immediate color change to deep purple was observed for this reaction upon addition of the potassium acetate base, a reaction time of 3 days was required to fully convert all species to the acetate complex and ensure complete consumption of the [Ru(trpy)(NIL)(Cl)]$^+$ species, the latter being an intermediate that is easily detected by mass spectrometry. All complexes display good solubility in polar solvents such as acetone, methanol, and acetonitrile; however, the acetate ligand in complexes **3**−**9** readily dissociates in acetonitrile and methanol, hence their studies are here restricted to acetone solutions. All complexes are characterized as diamagnetic based on the fact that they exhibit ^{1}H NMR spectra without unusual shifts or line broadening. This behavior is in agreement with the previous literature report of the chloride complex **1** by Maji et al.[33] In contrast to the work of Maji et al., two structural isomers were observed for **1** (as well as for complexes **2**− **9**) in this study because of the unsymmetrical nature of the chelating 2-iminoquinone ligand. Efforts to separate both structural isomers were unsuccessful, making their ^{1}H NMR spectra very difficult to interpret. The structural isomers are designated *cis* and *trans* with respect to the position of the N−H group in relation to the chloride or acetate ligand (Figure 1). The N−H proton of both isomers is resolved and shifted downfield of the trpy and remaining 2-iminoquinone protons in the region 14−15 ppm. Our DFT calculations show the *cis* isomer to be more stable by up to 5 kcal mol^{-1} for acetate complexes **3**−**8** ; however, there is very little energy difference between the two isomers of the chloride complexes **1** and **2**. Because of the electronic and steric effects of the trifluoromethyl group of acetate complex **9**, the *trans* isomer is favored by over 2 kcal mol^{-1} (see Table 3 and Theoretical Calculation discussion below).

Electrochemistry. The redox processes for all complexes studied in this work and their corresponding data are shown in Scheme 3, Figures 2 and 3, and Table 1, respectively. In no case was it possible to observe either of the *cis* or *trans* structural isomers independently by cyclic voltammetry or square-wave voltammetry; however,

Scheme 3. One-Electron Redox Processes Observed for $[Ru^{II}(trpy)(NIL^{Ox})(X)]^+$ Systems (X = Cl^- or OAc^-)[a]

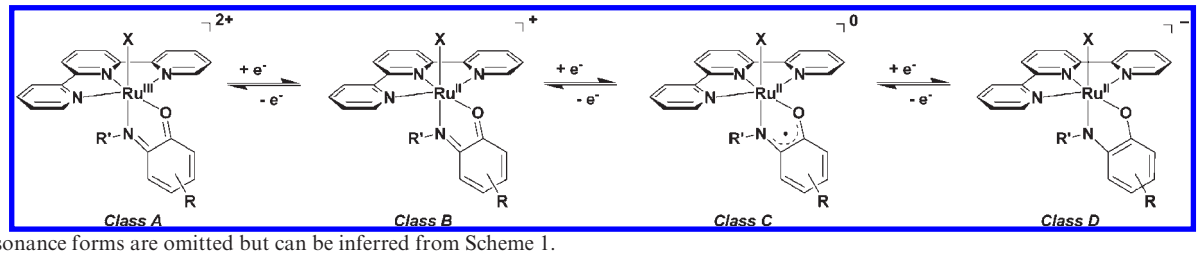

[a] Resonance forms are omitted but can be inferred from Scheme 1.

Table 3. Calculated Relative Free Energies (kcal/mol) in Acetone and in the Gas Phase (Parentheses) [a]

complex	*cis*-S	*cis*-T	*trans*-S	*trans*-T
1	0.59 (0.00)	8.27 (6.71)	0.00 (1.68)	9.19 (10.13)
2	0.55 (0.00)	9.12 (7.83)	0.00 (1.82)	9.78 (10.97)
3	0.00 (0.00)	8.87 (9.72)	3.00 (6.48)	12.17 (15.33)
4	0.00 (0.00)	9.59 (10.01)	3.04 (6.46)	12.04 (14.88)
5	0.00 (0.00)	9.12 (9.43)	3.15 (6.68)	11.84 (14.72)
6	0.00 (0.00)	10.25 (8.11)	5.04 (5.93)	12.87 (13.57)
7	0.00 (0.00)	7.95 (8.80)	2.91 (6.41)	10.53 (13.62)
8	0.00 (0.85)		0.83 (0.00)	
9	2.17 (3.26)		0.00 (0.00)	

[a] S and T represent the closed-shell singlet $Ru^{II}-NIL^{Ox}$ and open-shell triplet $Ru^{III}-NIL^{\bullet}$ configurations respectively.

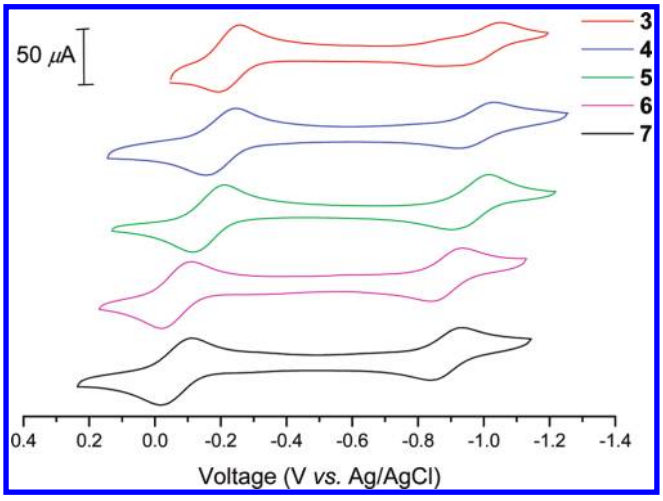

Figure 2. Cyclic voltammograms of acetate complexes **3**−**7** (1 mM in 0.1 M Bu_4NPF_6 acetone) showing successive one-electron reductions of the NILs (scan rate 50 mV s^{-1}).

non-Nernstian behavior of some redox process, for example, large peak separation (ca. 100 mV) and broad anodic and cathodic waves, of some of the complexes was attributed to the presence of both isomers in solution.

Chloride complexes **1** and **2** as well as the acetate complexes **3**−**7** display two irreversible one-electron oxidation events in the range +1.13 to +1.38 V and +1.26 to +1.41 V versus Ag/AgCl assigned to the $Ru^{III/II}$ and $Ru^{IV/III}$ couples, respectively. The redox potentials for **1** are in good agreement with the previous literature values;[33] however, our assignments differ. We reassign this species as being predominantly $Ru^{II}-NIL^{Ox}$ (not $Ru^{III}-NIL^{\bullet}$) in nature based on theoretical calculations and experimental UV−vis spectra (see the detailed discussion in the UV−vis Absorption and Spectroelectrochemistry and Theoretical Calculations sections). The values for the $Ru^{III/II}$ and $Ru^{IV/III}$ couples quoted in

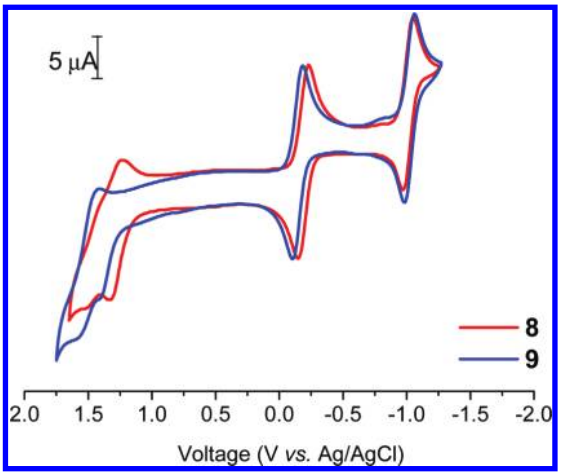

Figure 3. Cyclic voltammograms of *N*-aryl acetate complexes **8** and **9** (1 mM in 0.1 M Bu_4NPF_6 acetone).

Table 1 for complexes **1**−**7** were taken from square wave voltammograms and are here suggested as approximate values because of their irreversible character. The irreversible nature of these couples is explained by oxidative dehydrogenation of the N−H group on the 2−iminoquinone ligand in accordance with previous literature reports.[46−48] In contrast, the *N*-aryl complexes **8** and **9**, which preclude oxidative dehydrogenation, display quasi-reversible waves for the $Ru^{III/II}$ couple (Figure 3). Complex **9** has slightly more positive oxidation potentials (+1.38 V and +1.50 V for the $Ru^{III/II}$ and $Ru^{IV/III}$ couples, respectively) than **8** (+1.27 and +1.45 V) because of the electron withdrawing trifluoromethyl substituent on the *N*−aryl substituent.

Each complex also exhibits two redox processes at potentials more negative than their respective rest potentials, and these are assigned as sequential one-electron ligand-centered reduction processes (Figure 2 and Table 1). The first reduction occurs in the potential range −0.06 to −0.27 V versus Ag/AgCl, depending on the electron withdrawing *or* donating effect of the NIL substituent, and is a fully reversible process assigned to the $NIL^{Ox/\bullet}$ couple with formation of the neutral Class C species $[Ru^{II}(trpy)(NIL^{\bullet})(OAc)]^0$ (Scheme 3). Indeed the assignment of this redox couple is further corroborated in the UV−vis spectroelectrochemical and theoretical studies discussed below. The second reduction, also ligand

(46) Hoshino, Y.; Okuyama, F.; Nanba, A.; Shimizu, K.; Sato, G. P. *Bull. Chem. Soc. Jpn.* **1992**, *65*, 876–881.
(47) Gupta, N.; Grover, N.; Neyhart, G. A.; Singh, P.; Thorp, H. H. *Inorg. Chem.* **1993**, *32*, 310–316.
(48) Majumdar, P.; Falvello, L. R.; Tomas, M.; Goswami, S. *Chem.—Eur. J.* **2001**, *7*, 5222–5228.

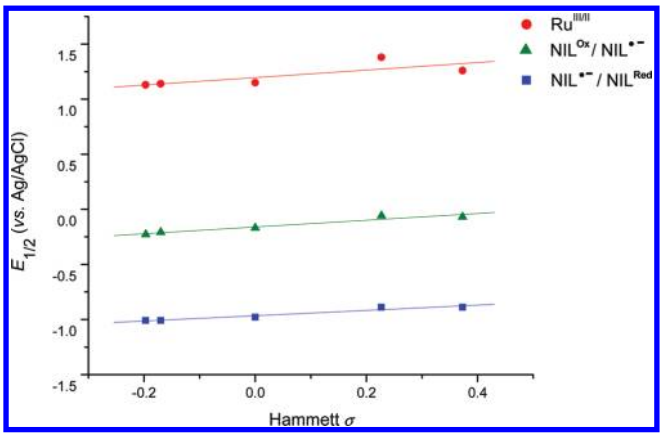

Figure 4. Hammett plots of reduction potentials for complexes **3**−**7**. Least squares analysis gives slopes of 0.34, 0.31, and 0.24 for the $Ru^{III/II}$, $NIL^{Ox/\bullet}$, and $NIL^{\bullet/Red}$ couples, respectively.

based, occurring in the potential range −0.86 to −1.05 V versus Ag/AgCl, is a quasi-reversible process assigned to the $NIL^{\bullet/Red}$ couple with formation of the formally negatively charged Class D $[Ru^{II}(trpy)(NIL^{Red})(OAc)]^-$ species (Scheme 3). Further reduction of the trpy ligand is anticipated for these complexes at more negative potentials; however, this process is not observed within the acetone potential window.

Class B Ru−NIL complexes are known to show parallel slopes for Hammett plots of their first oxidation and reduction potentials because of the extensive Ru(dπ)−NIL(π*) mixing.[22,49] The reduction potential of the $NIL^{Ox/\bullet}$ couples all vary linearly with respect to the Hammett parameter (σ) of the substituents on the ligand (a range of 170 mV is observed for complexes **3**−**7**) with a concomitant anodic shift of the $Ru^{III/II}$ couple (Figure 4). A previous study by Wada et al. showed a greater ligand dependence for a series of $[Ru(trpy)(NIL)(OAc)]^0$ Class C dioxolene systems with a preference for the Ru^{III}−NIL^{Red} resonance form when the NIL is substituted with up to four Cl atoms.[32] The larger Hammet slopes observed for this series are explained by the dioxolene ligand having enhanced overlap with the Ru(dπ) system because of its greater electronegativity ($C_6H_4O_2$ > C_6H_4NHO > C_6H_4NHNH).[22−24,50] The $h\nu$(MLCT) − ΔE(redox) difference for complexes **1**−**9** is consistently within the range 0.7−0.9 eV, also indicative of a highly delocalized Ru-NIL structure.[24,26,51] Interestingly, the $h\nu$(MLCT) − ΔE(redox) difference increases with the electron withdrawing nature of the substituent corresponding to increased mixing of the Ru(dπ)−NIL(π*) orbitals and possibly greater Ru^{III}−$NIL^{\bullet}$ character. This trend is also borne out in the DFT studies. The calculated charge density of Ru and the NIL ligand is shown in Supporting Information, Figure S1, and qualitatively maintains a linear slope with respect to the various substituents on the NIL for both *cis* and *trans* isomers. Greater charge separation, that is, positive charge on Ru and negative charge on quinone, was predicted with increasing electron withdrawing ability of the substituted quinone ligand, thus indicating increased Ru^{III}−$NIL^{\bullet}$ character.

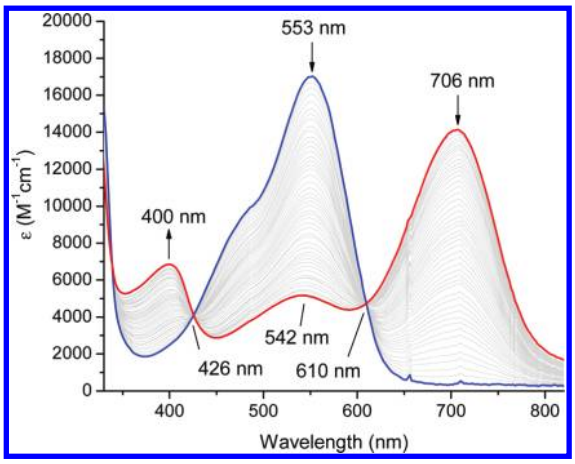

Figure 5. Overlay of UV−vis absorption spectra following the reduction of $[Ru^{II}(trpy)(NIL^{Ox})(OAc)]^+$ (**5**; blue) to form $[Ru^{II}(trpy)(NIL^{\bullet})(OAc)]^0$ (**5**$^-$;red) in acetone (0.1 M Bu_4NPF_6) with an applied potential of −0.40 V vs Ag/AgCl.

UV−vis Absorption and Spectroelectrochemistry. The occurrence of extensive Ru(dπ)−NIL(π*) mixing in Class B Ru−NIL species is characterized by intense low-energy bands that appear to have little charge transfer character, that is, only show weak solvatochromism. Complexes **1**−**9** are an intense purple/magenta color with a high molar absorptivity in the visible region (λ_{max}: 552−568 nm, ε: 1.51×10^4−1.92×10^4 M^{-1} cm^{-1}). While this broad (fwhm ~ 8×10^4 cm^{-1}) intense absorption is conveniently assigned to a $Ru^{II} \rightarrow NIL^{Ox}$ MLCT transition, the absorptions can be more accurately described as ML→ML transitions because of the nature of the extensive mixing of Ru(dπ)−NIL(π*) as previously described by Lever et al.[22−24] Comparable metal and ligand character of both HOMO and LUMO orbitals responsible for this transition impart very weak CT character as described in the Theoretical Calculations section below; however, the parallel slopes observed in the Hammet plots of the $Ru^{III/II}$ and $NIL^{Ox/\bullet}$ redox couples are consistent with the assignment of MLCT transitions (Figure 4). Therefore, we will employ the term MLCT to describe all these transitions with the understanding that in some cases the transition may be better described as ML→ML. Upon one-electron reduction of the NIL^{Ox} ligand by controlled potential electrolysis via the reaction $[Ru^{II}(trpy)(NIL^{Ox})(OAc)]^+ + e^- \rightarrow [Ru^{II}(trpy)(NIL^{\bullet})(OAc)]^0$, this electronic transition is significantly red-shifted. An example is shown in Figure 5 where, upon reduction of **5** to **5**$^-$ at an applied potential of −0.40 V versus Ag/AgCl (0.1 M Bu_4NPF_6 in acetone), the λ_{max} at 553 nm assigned to the $Ru^{II} \rightarrow NIL^{Ox}$ MLCT transition shows a dramatic decrease in intensity with a slight hypsochromic shift to 542 nm. This **5**$^-$ transition is composed of a mixture of electronic transitions, the most prominent being $NIL^{\bullet} \rightarrow$ trpy LLCT. Concurrently, an intense absorption grows in at lower energy having a λ_{max} at 706 nm assigned to the $Ru^{II} \rightarrow NIL^{\bullet}$ MLCT transition of the Class C $[Ru^{II}(trpy)(NIL^{\bullet})(OAc)]^0$ species **5**$^-$. The appearance of a band at 400 nm was also observed (assigned as $Ru^{II} \rightarrow$ trpy MLCT) as well as two isosbestic points at 426 and 610 nm indicative of a clean A → B

(49) Masui, H.; Lever, A. B. P.; Dodsworth, E. S. *Inorg. Chem.* **1993**, *32*, 258–267.
(50) Masui, H.; Lever, A. B. P.; Auburn, P. R. *Inorg. Chem.* **1991**, *30*, 2402–2410.
(51) *Inorganic Electronic Structure and Spectroscopy*; Lever, A. B. P., Dodsworth, E. S., Eds.; Wiley: New York 1999; Vol. *2*.

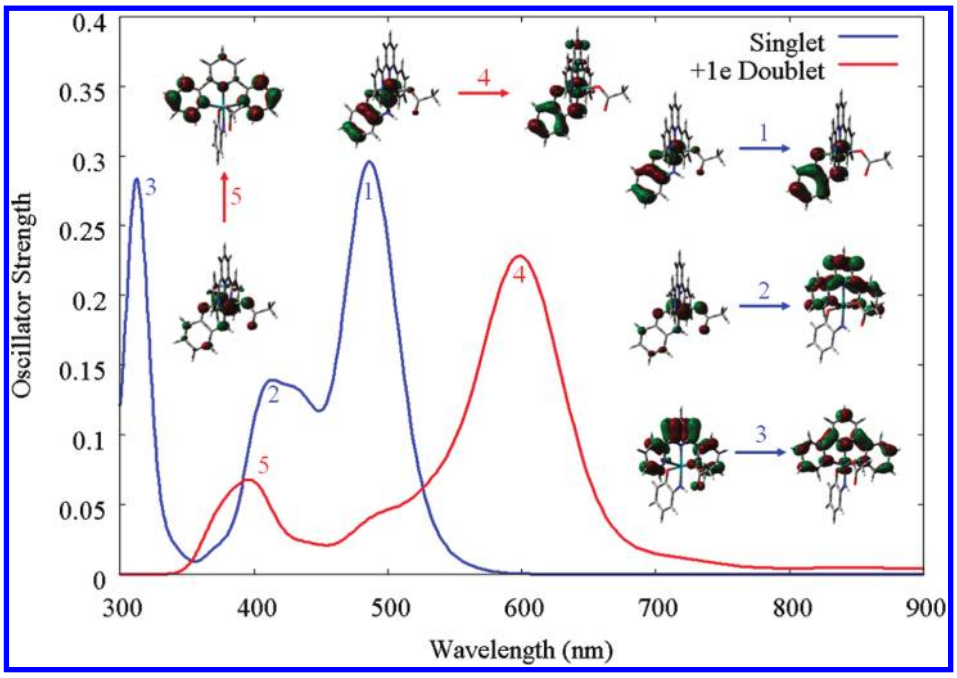

Figure 6. Calculated UV−vis spectra in acetone solution of the *cis* forms of **5** and $\mathbf{5}^-$ with the molecular orbitals principally involved in each transition (isodensity = 0.04).

process. The corresponding calculated spectra in acetone are shown in Figure 6 and show good agreement with the absorption patterns of the two species, but the calculated spectra are blue-shifted by about 100 nm as is typical for TD-DFT calculated MLCT bands. Further one-electron reduction of $\mathbf{5}^-$ via the $NIL^{\bullet/Red}$ redox process was also achieved upon an applied potential of −1.20 V versus Ag/AgCl. The decrease and increase in intensities of a 706 nm band and about 430 nm absorption, respectively, correlates to spectral changes observed for the change from $Ru(trpy)(NIL^{\bullet})(CO)^{+}$ to $Ru(trpy)(NIL^{red})(CO)$ where NIL = benzoquinone.[52] The experimental and calculated spectra of the fully reduced species is less characteristic, as the electron rich Class D $[Ru^{II}(trpy)(NIL^{Red})(OAc)]^{-}$ species contains fully reduced metal and ligand centers (Supporting Information, Figure S2 and S3).

Theoretical Calculations. The calculated relative free energies of the complexes are tabulated in Table 3. The ground states of the geometry-optimized *cis* and *trans* isomers are all closed-shell singlet $Ru^{II}-NIL^{Ox}$, and all attempts to locate open-shell singlet $Ru^{III}-NIL^{\bullet}$ configurations using the BS-DFT approach collapsed back to the closed-shell configuration. Each of the $Ru^{III}-NIL^{\bullet}$ open-shell triplet states is significantly higher in energy than the corresponding closed-shell singlet configurations causing the open-shell singlet state to be unstable under the unrestricted molecular orbital scheme. The chloride complexes, **1** and **2**, favor the *cis* form in the gas phase, but the *trans* forms, owing to their larger dipole moments, are lower in energy in acetone solution by less than kT. Therefore, both isomers are expected to be populated experimentally. The *cis* isomer is favored for complexes **3**− **7**, indicating that the more electronegative O atom of the NIL prefers the *trans* position. In complex **8** the difference in energy of the two isomers is much smaller owing to the steric repulsion arising from the phenyl group on the imino N, but the greater dipole of the *cis* isomer stabilizes it in solution. The trifluoromethyl-phenyl group on the imino N introduces so much steric repulsion that the less crowded *trans* position is favored for **9**.

Having established the formation of the Class B and Class C species, $[Ru^{II}(trpy)(NIL^{Ox})(OAc)]^{+}$ and $[Ru^{II}(trpy)(NIL^{\bullet})(OAc)]^{0}$ through both experimental and theoretical correlations, one must address the issue of spin states of the species involved. As mentioned earlier, Class B complexes **1**−**9** are all diamagnetic as evidenced by the fact that they exhibit ^1H NMR spectra without unusual shifts or line broadening. This assumption is in agreement with the conclusions of Maji et al.[33] Although diamagnetic with a charge of +1, the spin states of this class of complexes have been in question because of the ambiguous distribution of the electron density over the Ru−NIL framework. Maji et al. assigned complexes **1** and **2** as being predominantly the spin-coupled open-shell singlet $Ru^{III}-NIL^{\bullet}$ species with the unpaired spin-coupled electrons residing in localized orbitals on the metal center and NIL.[33] The antiferromagnetically coupled (open-shell) singlet $Ru^{III}-NIL^{\bullet}$ configuration for complexes **1**−**9** collapses back to the ground-state (closed-shell) singlet $Ru^{II}-NIL^{Ox}$ configuration when the BS-DFT approach is applied. This is interpreted to result from the strong coupling between the ruthenium and the NIL in these complexes such that pairing the frontier α and β valence electrons leads to the lowest electronic energy, instead of antiferromagnetically populating separate orbitals. On the basis of the DFT calculations on the Class B complexes listed in Table 3, we assign all the complexes considered in this work to be predominantly the closed-shell singlet $Ru^{II}-NIL^{Ox}$ species. Furthermore, the one-electron-reduced species can be unambiguously assigned as the doublet $Ru^{II}NIL^{\bullet}$ species,

(52) Wada, T.; Fujihara, T.; Tomori, M.; Ooyama, D.; Tanaka, K. *Bull. Chem. Soc. Jpn.* **2004**, *77*, 741–749.

and the two-electron reduced species to the singlet Ru^{II}-NIL^{Red} species. Our assignment of the doublet one-electron-reduced species is in agreement with Maji et al., who showed unequivocally via EPR analysis that the unpaired electron is localized on the ligand to make complex **1**. It is important to realize, however, that this does not necessarily prove the predominant resonance form of the Class B precursor complex because reduction of either $Ru^{II}-NIL^{Ox}$ *or* $Ru^{III}-NIL^{\bullet}$ can yield the $Ru^{II}-NIL^{\bullet}$ product.

Figure 6 shows the calculated UV−vis spectra of **5** and its one-electron-reduced species $\mathbf{5}^{-}$ in acetone along with the molecular orbitals that are principally involved in each transition. The dominant visible peak in the calculated spectrum of **5** at 487 nm (cf., exptl. 553 nm) is predicted to shift to 600 nm (cf., exptl. 706 nm) upon reduction, in qualitative agreement with the experimental result. While the calculated peaks are shifted to the blue (which is common when comparing the charge transfer bands of TD-DFT results with experiment) by 66 and 106 nm, respectively, the shapes and heights of the calculated and experimental peaks are quite similar as mentioned in the UV-vis Absorption and Spectroelectrochemistry section. Both these peaks are calculated to arise from ML → ML transitions.

X-ray Crystallography. The bond lengths in the NIL^{Ox}, $NIL^{\bullet}$, or NIL^{Red} ligands can themselves be very characteristic of the electronic environment of the metal center and are often used in assigning its formal oxidation state in combination with theoretically calculated bond distances.[53] For the specific case of Ru−NIL systems, however, which exhibit extensive orbital mixing across the metal−ligand framework, assignment of formal oxidation states based on localized bond distances alone may lead to ambiguous results. In fact, the majority of Class B systems, which are predominantly of the $Ru^{II}-NIL^{Ox}$ configuration, display bond lengths typical of the $NIL^{\bullet}$ oxidation state because of this extensive delocalization.[26]

Selected bond lengths and angles are summarized in the Supporting Information, Table S1. All bond lengths and angles observed here are comparable to similar systems reported in the literature, but a few noteworthy differences between the two isomers **2t** and **2c** are brought to light here.[26] Interestingly, the Ru−N(1) bond lengths are almost identical in the *cis* and *trans* isomers [1.980(10) Å and 1.961(6) Å, respectively], and so are the Ru−O(1) bond lengths [2.073(10) Å, 2.069(6) Å, respectively]. A nearly identical bite angle of the 2-imino-4-^{t}butylquinone ligand is also observed (79.4(4)° and 78.9(3)° in the *cis* and *trans* isomers, respectively) giving rise to Cl−Ru−O(1) and Cl−Ru−N(1) *trans*-angles of 174.4(2)° and 169.7(2)° for the *cis* and *trans* isomers, respectively. There is a longer Ru−Cl bond length in the *trans* isomer [2.380(3) Å] which is expected because of the increased back-donation of N(1), as opposed to O(1) in the *cis* isomer [2.360(4) Å]. A similar effect is observed in the Ru−N(21) [1.998(9) Å, 1.966(7) Å, respectively] bond lengths of the *cis* and *trans* isomers.

For the 2-imino-4-^{t}butylquinone ligand in complex **2** the bond distances vary between the two isomers as shown in Figure 8. Typical bond distances for $Ru^{II}-NIL^{Ox}$ and $Ru^{III}-NIL^{\bullet}$ are reported to be as follows: C═O, 1.22 and 1.30 Å; C=NH, 1.31 and 1.35 Å; C1−C2, 1.48, and 1.43 Å; C4−C5, 1.45, and 1.42 Å, respectively.[53] Bond distances for **2c** and **2t** lie somewhere between the $Ru^{II}-NIL^{Ox}$ and $Ru^{III}-NIL^{\bullet}$ configurations. For this reason, in addition to theoretical methods

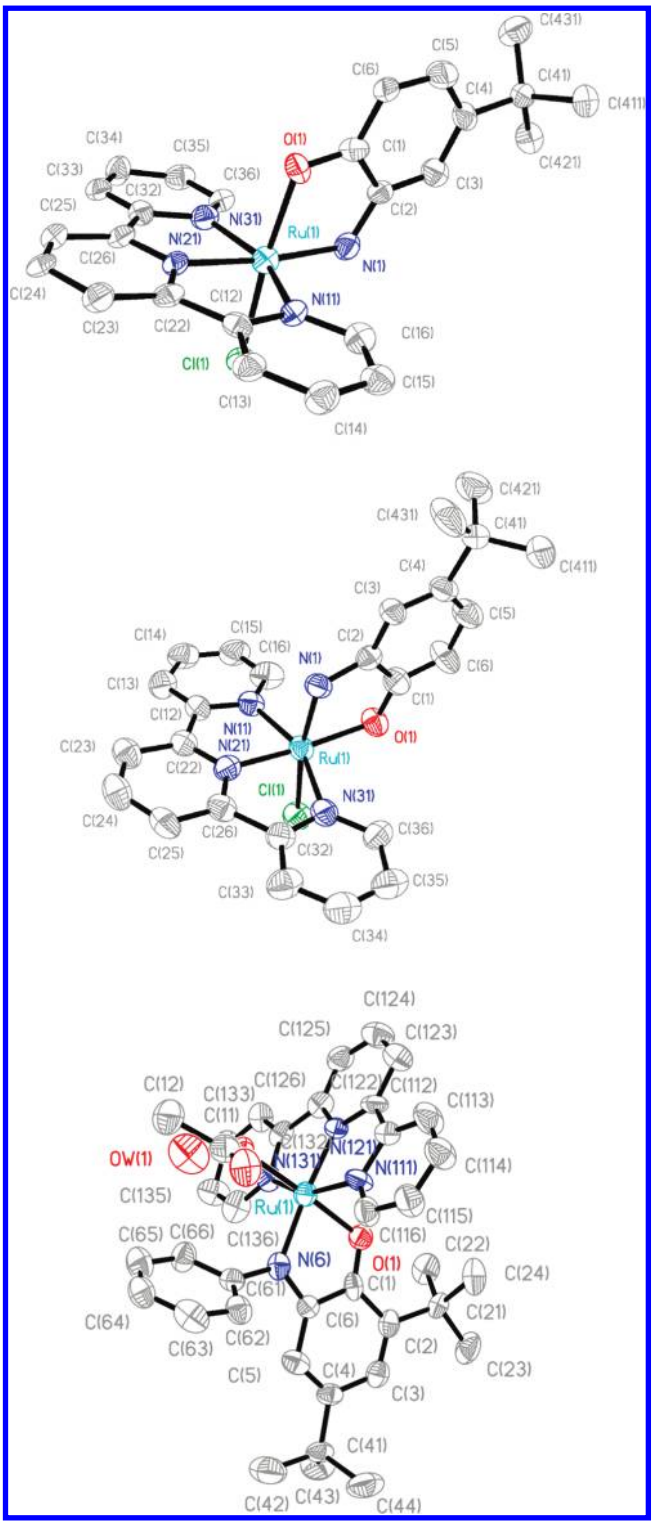

Figure 7. ORTEP plots of **2c** (top) and **2t** (middle) isomers of [Ru(trpy)(4-^{t}BuC$_6$H$_3$NHO(Cl)]ClO$_4$, and **8c** (bottom). Non-coordinating anions and solvent molecules are omitted.

(53) Bhattacharya, S.; Gupta, P.; Basuli, F.; Pierpont, C. G. *Inorg. Chem.* **2002**, *41*, 5810–5816.

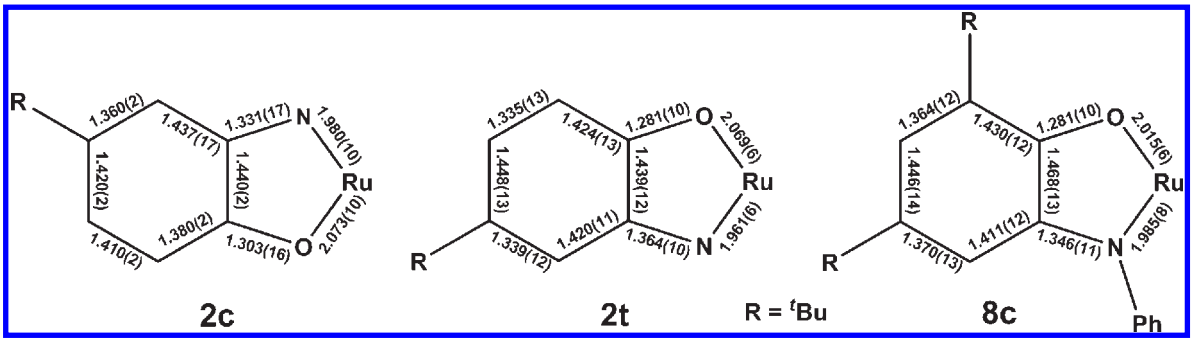

Figure 8. Experimental bond distances observed by single-crystal X-ray crystallography for the $Ru^{II}-NIL^{Ox}$ metallocycle fragment of **2c** (left), **2t** (middle), and **8c** (right).

discussed earlier, it can be understood why the $[Ru^{II}(trpy)(NIL^{Ox})(Cl)]^+$ complex was previously interpreted by Maji et al. as having the $[Ru^{III}(trpy)(NIL^{\bullet})(Cl)]^+$ configuration.

Although two isomers for **8** were observed in the ^1H NMR spectrum, the *cis* isomer preferentially crystallized from solution with one water of hydration hydrogen bonded to the acetate ligand (Figure 7, bottom). The assignment of the ligand oxidation state based on X-ray crystallography data alone is again ambiguous (Figure 8). As mentioned above, the bond distances for NIL lie between literature values for NIL^{Ox} and $NIL^{\bullet}$ oxidation states.[53] DFT calculations predict the closed-shell singlet states as ground states for **2c**, **2t**, and **8c**. Attempts to optimize the open-shell singlet configuration through BS-DFT calculations for **8c** converged back to the closed-shell singlet configuration. Therefore, we assigned **2c**, **2t**, and **8c** as having a predominantly $Ru^{II}-NIL^{Ox}$ configurations, even though the X-ray single-crystal data are ambiguous.

Conclusions

The metal and ligand oxidation states of a series of $[Ru(trpy)(NIL)(X)]^n$ complexes ($X = Cl^-$ *or* OAc^-; $n = +1, 0$) have been investigated by a combination of spectroscopic, electrochemical, and theoretical techniques. The assignment of oxidation states and spin states for these systems is not trivial and is often ambiguous. In some cases they have been misassigned. Complexes **1**−**9** display two successive one-electron reductions negative of their respective rest potentials that are assigned as the $NIL^{Ox/\bullet}$ and $NIL^{\bullet/Red}$ redox couples. Control of these redox couples was demonstrated by a Hammet σ versus $E_{1/2}$ plot, which correlated well with the trend in Mulliken charge population at the Ru and NIL moieties observed by DFT analysis. Although observed crystallographic bond lengths suggest some $Ru^{III}-NIL^{\bullet}$ character, all attempts to locate the open-shell singlet $Ru^{III}-NIL^{\bullet}$ configurations using the BS-DFT approach collapsed back to the closed-shell configuration $Ru^{II}-NIL^{Ox}$. We believe that a better understanding of electronic structures can be achieved for these systems by using a combination of electrochemical, spectroscopic, X-ray crystallographic, and theoretical methods. However, we should add that standard DFT calculations could mislead the assignments.

Acknowledgment. The work at Brookhaven National Laboratory is funded under contract DE-AC02-98CH10886 with the U.S. Department of Energy and supported by its Division of Chemical Sciences, Geosciences, & Biosciences, Office of Basic Energy Sciences. Computational resources were provided by the National Energy Research Scientific Computing Center, which is supported by the Office of Science of the U.S. Department of Energy and the New York Center for Computational Sciences (New York Blue). The authors also thank the U.S. Department of Energy for funding under the BES Hydrogen Fuel Initiative.

Supporting Information Available: Table of selected bond distances and angles for **2c**, **2t**, and **8c**, plot of Hammet σ parameters versus calculated Mulliken charge densities of Ru and NIL fragments, calculated dipoles and Mulliken charge densities of Ru and NIL fragments, UV−vis absorption spectrum of $\mathbf{5}^{2-}$, and optimized geometries of complexes **1**−**9**. This material is available free of charge via the Internet at http://pubs.acs.org.